Journal of Biomedical Optics 6(3), 292–299 (July 2001)

Spatially modulated illumination microscopy: online visualization of intensity distribution and prediction of nanometer precision of axial distance measurements by computer simulations

B. Albrecht
A. V. Failla
Kirchhoff Institute for Physics (KIP)
University of Heidelberg
Applied Optics & Information Processing
D-69120 Heidelberg, Germany

R. Heintzmann
Max-Planck-Institute for Biophysical Chemistry
D-37077 Göttingen, Germany

C. Cremer
Kirchhoff Institute for Physics (KIP)
University of Heidelberg
Applied Optics & Information Processing
D-69120 Heidelberg, Germany
and
University of Heidelberg
Interdisciplinary Center for Scientific Computing (IWR)
INF 368, D-69120 Heidelberg, Germany

Abstract. During the last years, measurements considerably beyond the conventional "Abbe-Limit" of optical resolution in far field light microscopy were realized by several light microscopical approaches. Point spread function (PSF) engineering, spectral precision distance microscopy (SPDM), and related methods were used to demonstrate the feasibility of such measurements. SPDM allows the measurement of position and multiple distances between point-like fluorescent objects of different spectral signatures far below the optical resolution criterion as defined by the full width at half maximum of the PSF. Here, we report a software method to obtain online visualization of light distribution in the lateral and axial direction of any object detected in a spatially modulated illumination (SMI) microscope. This strongly facilitates routine application of SMI microscopy. The software was developed using Microsoft Visual C++ running on Windows NT. Furthermore, some aspects of the theoretical limits of the SPDM method were studied by virtual microscopy. For the case of SMI microscopy the precision of axial distance measurements was studied, taking into account photon statistics and image analysis procedures. The results indicate that even under low fluorescence intensity conditions typical for biological structure research, precise distance measurements in the nanometer range can be determined, and that axial distances in the order of 40 nm are detectable with such precision.
 [DOI: 10.1117/1.1383293]

Keywords: spatially modulated illumination (SMI) microscopy; hardware control; object oriented programming; visualization; virtual microscopy; computer simulations.

Paper FM-07 received Apr. 10, 2001; revised manuscript received May 2, 2001; accepted for publication May 4, 2001.

1 Introduction

In many far field light microscopical applications in the life sciences, it is important to measure positions and mutual distances between fluorescent objects situated in thick transparent specimens with high precision. For example, this allows to study genome nanostructure in three-dimensionally (3D) intact cell nuclei.[1–3] The objects are labeled with fluorescent markers having different spectral signatures.[4,5] This allows one to identify the objects due to their excitation/emission spectra, or fluorescence lifetimes. The object positions and their mutual distances are then determined from their coordinates in the image data file, e.g. with respect to a given cover slip position (spectral precision distance microscopy (SPDM) and related methods).[1,2,6–9]

Typically, measurements of small fluorescence labeled biological objects[2,6] have to be performed under conditions of low fluorescence photon statistics which lead to a restricted accuracy in the determination of their distances. To achieve distance determinations with a precision (standard deviation of the mean distance) in the nanometer range, in addition to the general SPDM approach, methods of ''point spread function engineering'' are required. Their goal is to modify the point spread function (PSF) of the microscope system (corresponding to the image of a fluorescent ''point-like'' object) in such a way that a given total fluorescence photon count results in a maximum precision of position determination of the object.

Here, we describe the experimental setup and the software to perform such measurements for the determination of axial distances between subwavelength sized objects. In the examples shown here, beads were used. In its main part the experimental setup consists of a spatially modulated illumination (SMI) microscope. Here, the object is placed between two objectives and is illuminated by two coherent laser beams of the same intensity which counterpropagate in the object space.[10–12] During the measurements, the object slide is moved step-by-step along the axial direction; at each position

Address all correspondence to C. Cremer. E-mail: christoph.cremer@kip.uni-heidelberg.de

1083-3668/2001/$15.00 © 2001 SPIE

a 2D image (optical section) is taken by a charge-coupled device (CCD) camera.

The software for the control of this process was developed using the development environment ''Visual C++, Version 6.0'' from Microsoft. For practical reasons we decided to realize this project in an object oriented way. Besides controlling of the measuring process, this new application allows the visualization of the collected experimental data stacks immediately after the measurement. Therefore a direct and fast interpretation of the data by the operator of the system is possible.

In addition, we describe the theoretical shape of the SMI PSF and the principle of the high precision distance determination. This is followed by a characterization of the SMI virtual microscopy simulations and their results.

2 Microscopical Setup

The general design of the microscopical SMI setup used here has been described elsewhere.[11–13] Briefly, in its central part it consists of a rectangular interferometer stretched by a 50:50 beam splitter. Each of the two collimated, vertically polarized laser beams for the fluorescence excitation has a diameter of about 15 mm and is focused into the back focal plane of two opposite objective lenses. This configuration leads to a ''standing wave field'' between the objectives with plane waves and a $\sin^2$ modulation of the laser intensity along the axial direction; it is called the illumination point spread function (illumination PSF).

The objects which are situated in the space between the two opposite objective lenses are mounted between a conventional object slide and a cover slip. As mentioned above, to carry out the measurements they can be moved along the axial direction (providing optical sectioning) using a piezoelectric stage; alternatively, the phase of the standing light field can be varied by a piezoelectrically adjustable mirror. The minimal step size of the object stage is 10 nm; that of the mirror stage is 1 nm; the position resolution is 1 and 0.05 nm, respectively. The piezoelectric object stage itself is attached to a stepper motor powered object stage for the macroscopic movement of the object slide; this provides lateral translation for searching for suitable objects and moving the object slide in or out of the interspace between the objectives.

For the detection of the emitted fluorescence light, on one side between the focusing lens and the objective, one mirror is replaced by a dichroic beamsplitter. Since the objectives were designed according to infinite optics, the collimated detection light beam is focused onto the CCD chip of a cooled color CCD camera by a respective tube lens. The detection light path is the same as in an epifluorescence microscope. Consequently, the effective PSF of the system is given by the product of the illumination PSF and the detection PSF; the latter corresponds to the PSF in the epifluorescent microscopy case (compare Figure 4 for an experimental example). In order to improve contrast, a blocking filter is installed in front of the camera to prevent passing of residual excitation light.

The CCD camera is connected via a fiber optical link to a PCI board in a personal computer (PC) which is running under Windows NT. The control boxes of the stepper motors and the piezo stages are connected to the same PC via serial ports.

For excitation both an Ar^+ laser ($\lambda_{ex}=488$ nm) and a Kr^+ laser ($\lambda_{ex}=647$ nm) were used. The laser light is guided to the SMI microscope via two polarization-conserving single-mode glass fibers. Before entering the interferometer of the SMI microscope, the two beams are merged by a beam combiner. The whole setup is mounted on a breadboard made of superinvar to minimize thermally induced shifts of the optical components. The optical axis of the two objective lenses has a horizontal orientation, whereas the object slide has a vertical orientation. As objects, we used PS- and TetraSpeck-beads (Molecular Probes) with several diameters embedded in Vectashield mounting medium. Figure 1 shows a 3D representation of a typical 3D-image stack.

3 Setup Control

3.1 Structure of the Software

Since the software and the source code of the application, respectively, have an object oriented structure, the structure of the experimental setup can be retrieved in the source code again. This means that each physical object (CCD camera, stepper motor control box, piezo control box) is associated with its own software object. Thus the task for each of these software objects is to control only the respective hardware object. These control software objects provide certain functions and methods which are called from other user interface objects. The user interface objects provide the interaction with the user. Therefore each control software object is associated with its own hardware object on the one side and its own user interface object on the other side. The user interface objects again are represented by dialog boxes visible to the user.

All these objects in turn are embedded in one object which represents the main window of the application. Aside from this, there are more objects, e.g. for displaying the histogram or the profiles (see below). The whole structure of the application follows the so-called document/view architecture, i.e. objects containing ''document data'' and respective hardware control methods are separated from objects providing interac-

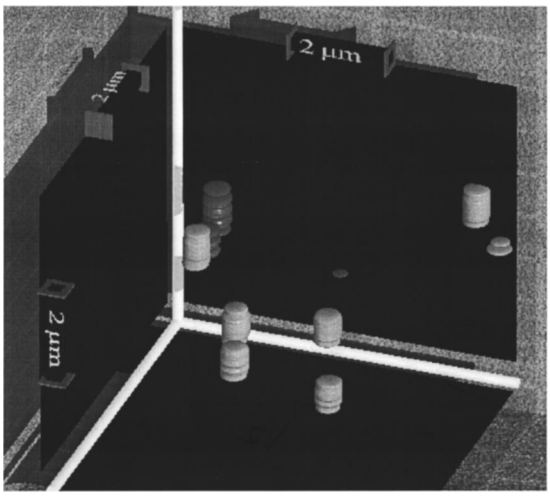

Fig. 1 3D representation of a SMI measurement of yellow-green and dark red PS beads with a diameter of 170 nm illuminated with two laser lines (λ=488 and 647 nm).

tion with the user and representation of the document data. For more details see Refs. 14–16 or the documentation of Microsoft's Visual C++, Version 6.0.

3.2 Hardware Control and Real-Time Visualization

The task of the control software is, apart from providing the visualization of the measured data, to control and coordinate all electronic components, i.e. stepper motors, CCD camera, and piezo stages.

As mentioned above, the stepper motors are used for macroscopic translations of the object slide. This can be done by manually actuating a joystick attached to the control box of the stepper motors. Nevertheless, control by the PC is required: It is used to set the speed and software limits of the moving area of the stepper motors. The latter is needed in order to avoid a crash of the object slide on the objectives. Furthermore, the stepper motors can be prompted by the PC software to move the object slide to certain positions manually put in or assigned before. Finally, the joystick can be deactivated to avoid unintended moving of the object stage, for example during the measuring process (see below).

For the microscopic positioning of the object slide, the piezo driven object stage is applied. The position of this stage as well as the position of the piezoelectrically driven mirror stage can be varied by manually actuating the positions of two slides displayed in a dialog box of the control software. During the performance of the measuring process, either the position of the object stage or the position of the mirror stage is automatically set.

Two important parameters of the CCD camera are the integration time and the region of interest (ROI). We can distinguish two camera operation modes: In the first mode, a short integration time is set (about 100 ms) and the entire CCD chip is used for acquisition; i.e. the ROI is equal to the entire CCD chip. This mode is used for real-time visualization of the objects on the object slide and thus for the search of objects which seem to be suitable for the three-dimensional (3D) acquisition and measuring process. When such objects have been found, the second mode is applied: To save memory, an ROI around the objects is defined; usually we choose a size of 64×64 or 128×128 pixels. Generally, the size of the ROI can be set arbitrarily. Furthermore, the integration time is increased up to typically 500 ms to improve photon statistics. During the real-time visualization, a histogram of the image data can be displayed which is also updated in real-time (see Figure 2).

3.3 Acquisition Process

Afterwards, the acquisition process can be started. Before doing this, some further parameters can be set or modified. This means that the scan mode (object or mirror scanning), step size and start and end positions of the chosen piezo stage, and the number of images to acquire had to be specified. Additionally, in order to perform repetitive measurements, the number of repetitions of the acquisition process can be set.

After switching the application into the acquisition mode, i.e. starting the acquisition process, the object itself, or the phase of the standing light field, is successively moved to the defined positions. At each position a 2D image (compare Figure 3) is taken by the CCD camera and stored one after another in the PC memory. Consequently, a 3D-image stack containing the axial intensity distribution of the objects in the third dimension is produced. Usually, we select 300–400 2D images and a step size of 20 nm. The total acquisition time for one 3D image takes about 2 min in the present scenario.

4 Visualization of the Axial and Lateral Intensity Distribution (Profile)

After the acquisition procedure is finished, the application switches into the display mode as shown in Figure 3 (main window of the control software). Here, a display of a lateral, two-dimensional optical section of a 3D data stack with a number of fluorescent objects (beads) can be seen [current (2D-) image]. The icons on the lower side of the window provide some basic actions of the program like loading or saving program parameters or image data and display dialog boxes for hardware control (CCD camera, stepper motors, piezo stages). Besides this, dialog boxes indicating the histogram of the displayed optical section and displaying of the axial or lateral intensity distribution and statistical parameters can be shown. The buttons on the left side can be used to load parameters from PC memory to the camera and to switch the camera to real-time visualization, to start a new acquisition procedure, or to navigate through the recorded 3D-image stack.

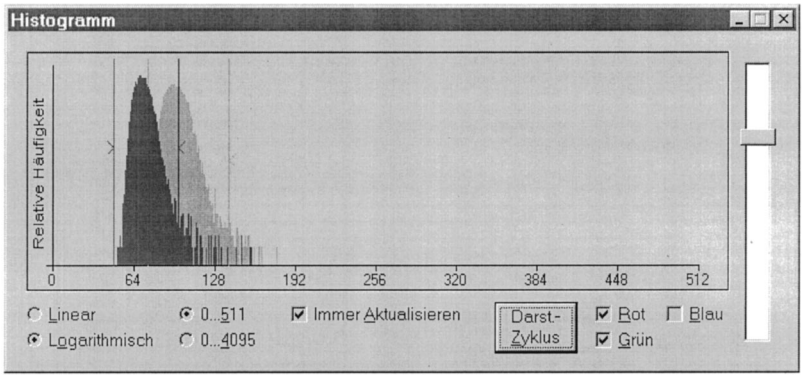

Fig. 2 Histogram of the currently displayed image data for red (left) and green channel (right). The markers indicate the intensity range displayed in the main window of the software (Figure 3). To change this range, the markers can be shifted.

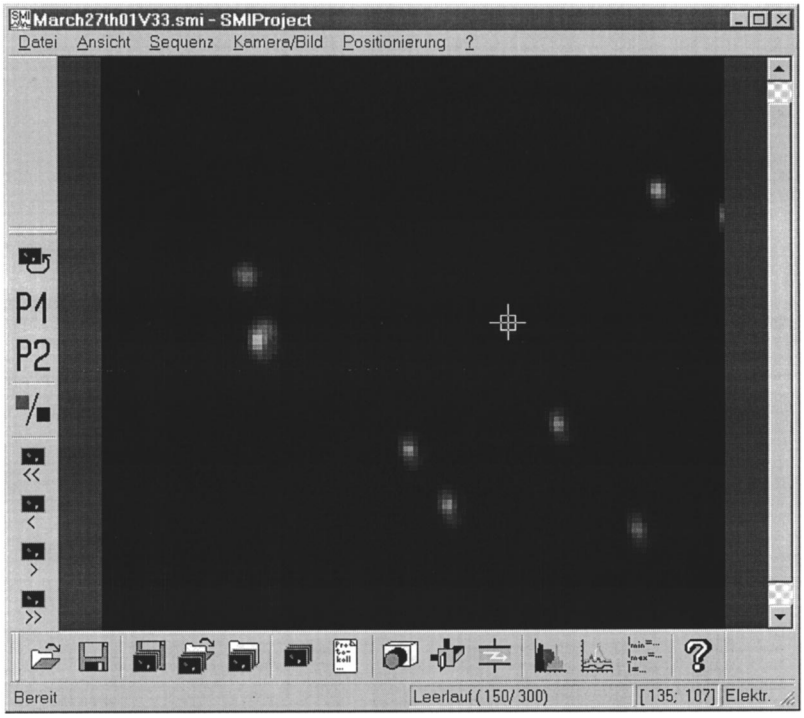

Fig. 3 Main window of the control software. The display shows one lateral 2D image (optical section) from the 3D-image stack presented in Figure 2 containing 300 2D images. The white square (ROI) can be moved by dragging the mouse; it specifies the region used for displaying the axial intensity distribution (*z* profile) through the image stack (compare Figure 4) or for indicating the region used for statistical evaluation.

By dragging the mouse over the currently displayed image, one can set the position of a ROI which is used to generate a 1D plot containing the axial (*z*) intensity distribution around its center: Every point of this plot corresponds to the intensity in the corresponding 2D-ROI image; its value is computed by calculating the mean intensity over the selected ROI; an option can be used to subtract from this the mean value over each entire 2D image. Additionally, one can select the size of the ROI (1×1, 2×2, pixels, ..., whole image) and decide for which of the three color channels of the CCD camera (red, green, blue) the axial intensity distribution is to be displayed. Figure 4 shows such a typical plot. The ROI marked on the current image can be used for statistical evaluation, too. In this case, the minimum and maximum intensity values and their respective coordinates in the image (stack) including the mean value and standard deviation of the selected region are calculated. The user can choose a color channel and decide whether to get the statistical values of the ROI in the current

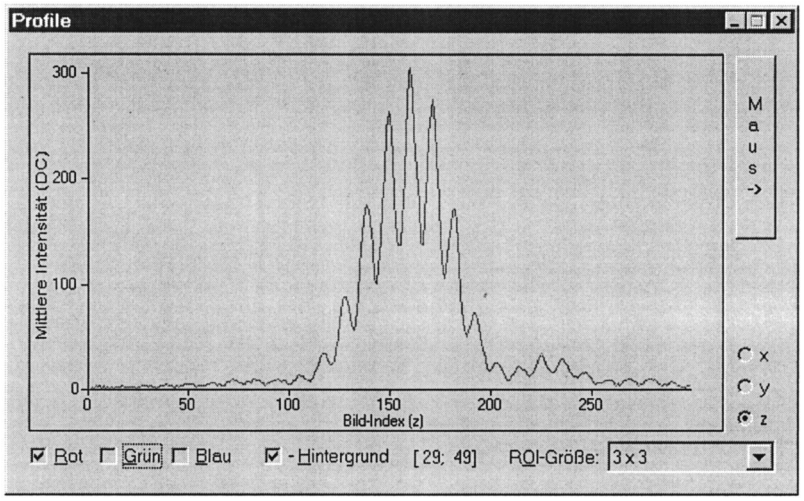

Fig. 4 Intensity distribution along the *z* direction (along the optical axis of the objective lenses). Each value in the graph relates to one 2D image (optical section) of the 3D-image stack and represents the mean value out of a ROI like that marked in Figure 3. Here, the axial intensity distribution of one PS bead at position (*x*=29; *y*=49), illuminated with one laser (λ=647 nm), along a 3×3 ROI is shown.

2D image or to take into account all 2D images of the whole 3D-image stack.

Alternatively, if "*x*" or "*y*" are chosen in the dialog box shown in Figure 4, one can define a horizontal or vertical line in the current image by dragging the mouse. In these modes, the corresponding *x* and respective *y* profile is displayed.

These online tools are very convenient to evaluate the acquired data. An important criterion is indicated by the modulation of the *z* profile curve (Figure 4). The modulation depends strongly on the object size. (1) If the object is too large, i.e. its diameter is much larger than the distance between two neighbored modulation fringes, the modulation is canceled out. In this case, the shape of the modulated axial intensity distribution merges into a conventional intensity distribution, like that in an epifluorescence microscope. (2) If the object size is considerably smaller than the fringe half-width, a strong modulation is obtained. Both computer simulations and experimental observations[17] indicated that by analysis of the modulation contrast (compare Figure 4), a size estimate considerably below λ/2 is possible.

5 Principle of Spatially Modulated Illumination Microscopy Distance Measurements

After the performance of the measuring process and selection of intensity distributions in regions of interest, the collected data are used to calculate the distances between the detected objects. To understand how to obtain the distance information from the data, a short description of the theoretical intensity distribution follows.

SMI microscopy is characterized by a fringe interference pattern produced by two laser beams focused into the back focal plane of two opposite objective lenses.[10,18] The PSF of this system can be written in the following way:

$$\mathrm{PSF}_{\mathrm{SMI}} = \mathrm{PSF}_{\mathrm{EPI}} \left(\cos \frac{2\pi n (z - z_0)}{\lambda} \right)^2, \tag{1}$$

where z is the axial coordinate, z_0 is a phase constant, λ is the wavelength of the excitation light, n is the index of refraction of the mounting medium, and $\mathrm{PSF}_{\mathrm{EPI}}$ is the epifluorescent PSF of a conventional light microscope. The axial SMI PSF (PSF_z) can be evaluated[18] and is given by

$$\mathrm{PSF}_z \approx A \left[\mathrm{sinc} \left(\frac{z - z_{\max}}{B} \right) \cdot \cos[K(z - z_0)] \right]^2, \tag{2}$$

where A is a positive constant, $z_{\max}$ is the position of the global maximum of the PSF_z, B is a constant proportional to the full width at half maximum (FWHM) of the epifluorescence PSF, and $K = 2\pi n(z - z_0)/\lambda$. It should be noted that the parameter z_0 contains information about the fringe oscillating pattern; thus it can be arbitrarily assumed to be equal to one of the relative maxima or minima positions of the PSF_z.

To obtain high precisions (standard deviations in the one nanometer range) in distance measurements, it is important to define respective distance determination algorithms. Let us call P_1, P_2 the two point-like objects; $z_{\max 1}$, $z_{\max 2}$, z_{01} and z_{02} are the values of the parameters $z_{\max}$ and z_0 relative to the point spread function of the two objects. Therefore the axial distance D_{21} between P_1 and P_2 can be defined in the following ways:

$$D_{21} = z_{\max 2} - z_{\max 1}, \tag{3}$$

$$D_{21} = z_{02} - z_{01}. \tag{4}$$

Both definitions are, theoretically, valid; moreover, the two procedures are the same if it is supposed that $z_{\max} = z_0$. But, from the practical and experimental point of view, while evaluating Eq. (4), the oscillation parameter is determined and all the axial data information is used. Instead, measuring $z_{\max}$ [see Eq. (3)], only the data in a small region around the global maximum of PSF_z (FWHM≈80 nm) have to be considered. Using the relation in Eq. (3), a lower precision in distance determination was observed (data not shown). In the following, only Eq. (4) will be used for the virtual evaluation of the SMI microscope precision in two point-like distance determination.

6 SMI Virtual Microscopy Simulations

The virtual microscopy simulations shown here were realized to study the precision limits in axial distance measurements of the SMI microscope due to photon noise and image analysis evaluation: To do so, the simulations were made varying the total number of photons detected per object; especially low photon counts conditions were analyzed.

Two independent point-like objects can be represented mathematically by two Dirac delta functions (the computer representation of a Dirac delta function is a voxel-like pulse with a maximum value equal to 255 in grayscale) situated in the position $\mathbf{P}_1(x_1, y_1, z_1)$,$\mathbf{P}_2(x_2, y_2, z_2)$ respectively:

$$P_{1(2)} = \delta(x - x_{1(2)}, y - y_{1(2)}, z - z_{1(2)}). \tag{5}$$

The objects visualized by two independent channels of the virtual SMI microscope are the results of the convolution of a Dirac delta function and the SMI PSF (see Figure 5). Thus the two independent point-like objects are represented by the SMI PSF centered in the points $\mathbf{P}_1(x_1, y_1, z_1)$ and $\mathbf{P}_2(x_2, y_2, z_2)$, respectively. The axial distance D_{21} between the two objects detected in the two independent channels was evaluated using an adaptation function in order to obtain z_{02} and z_{01}. The test adaptation function was given by the SMI PSF_z [see Eq. (2)], where A, B, K, z_0, and $z_{\max}$ were the unknown parameters of the fit.

In these simulations, a least-square fit algorithm was used. In each simulation the average total number N_{ph} of detected photons per object was fixed. The values determined were the mean and the standard deviation. Equation (4) was used after adding appropriate Poisson noise corresponding to the number N_{ph} of photons registered per object to each of the objects. This procedure was repeated 40 times with each "true" axial distance. Additionally, simulations were performed where N_{ph} was varied.

A different kind of simulation was realized (data not shown) taking into account the digitization procedure.[19] In this case the distance between the two points was not constant but changed every time in the following way:

$$D_{21i} = z_{02} + d_{2i} - (z_{01} + d_{1i}),$$
$$i = 1, \ldots, 40; \quad 0 \leq d_{1i} < 1; \quad 0 \leq d_{2i} < 1, \tag{6}$$

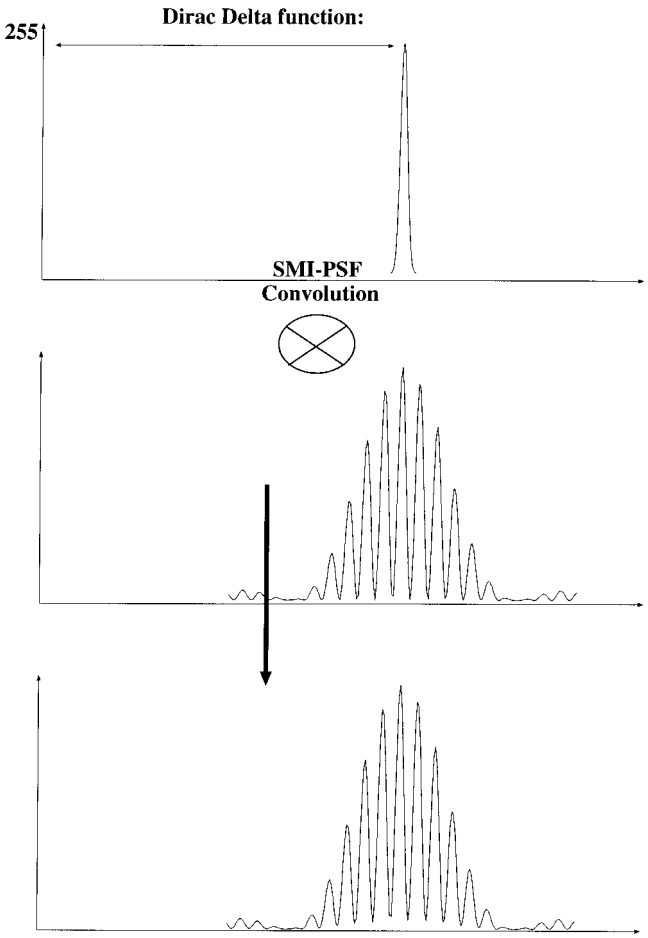

Fig. 5 Schematic example of SMI virtual microscopy: A point-like object (Dirac delta function visualized here by a narrow Gaussian) is convoluted with the SMI PSF.

where $d_{1(2)i}$ were produced by a random number generator. The evaluated distance D_d and its error ΔD_d were calculated in the following way:

$$D_d = \text{mean}(D_{21i}), \quad \Delta D_d = \sqrt{\frac{1}{40}\sum_{i=1}^{40}(D_{di} - D_{21i})^2}, \tag{7}$$

where D_{di} is the result of the fit evaluation of the true distance D_{21i}. The results of this kind of simulation will be published elsewhere.

7 Results of the Simulations

For these simulations the voxel sizes were chosen to be the same as in a real SMI microscope; here $100\times100\times20$ nm^2 were used. The ''true'' distances assumed were $D=600$ nm and $D=40$ nm, respectively. For calculating convenience, the two independent point-like objects, detected by two different channels, were supposed to have the same absorption/emission wavelength $\lambda=488$ nm (one of the wavelengths used in the real SMI microscope); such a condition may be experimentally realized, e.g. by fluorescence lifetime discrimination. In the simulation presented here, the FWHM of the PSF was equal to 600 nm and the FWHM of the oscillating fringes was equal to 80 nm. In Table 1 the mean detected distance values and their standard deviations are shown for several values of N_{ph}; the considered distances between the peaks were $D=40$ and $D=600$ nm.[20]

Table 1 Virtual axial SMI distance determination mean ± standard deviation (SD); the "true" distances D assumed between the two objects were 40 and 600 nm, respectively. The number N_{ph} of photons detected was assumed to be 125 and 65 000. For each distance n=40 object pairs were analyzed.

	SMI distance D_d/nm	
N_{ph}	D=600.0 nm	D=40.0 nm
125	599.7±6.8	38.8±8.5
250	601.1±4.3	39.6±5.5
500	600.4±3.1	39.1±3.8
750	599.5±2.8	40.7±3.3
1250	600.1±2.5	38.9±2.9
2500	599.7±1.3	40.5±1.8
5000	599.67±0.93	40.72±1.2
10 000	599.84±0.74	40.13±0.77
17 500	600.12±0.54	39.84±0.68
25 000	599.81±0.46	39.87±0.52
32 500	599.89±0.39	39.91±0.43
65 000	599.72±0.37	40.02±0.31

The data presented in Table 1 show that SMI microscopy allows to obtain axial distance measurements with high precision even if a low number of photons N_{ph} is detected. In fact, a total number of photons for each object detected equal to $N_{ph}=5000$ is sufficient to reach a precision of 0.9 nm.

In good agreement with other reports regarding both theoretical analysis and virtual microscopy simulations, the standard deviation in SMI distance determination is approximately proportional to $1/\sqrt{N_{ph}}$.[19] One may note, however, that the SMI virtual microscopy simulation allows one to give precise estimates of the standard deviations (SD) for each photon count N_{ph} in dependence of the special SMI-PSF and image analysis used. As expected, the SD strongly increases at lower photon counts, whereas for high photon counts the changes become extremely small (see Table 1).

SMI distance determination as described above for $D=600$ nm was carried out for $D=40$ nm, too. The results shown in Table 1 indicate that under the assumptions made, no significant differences in the standard deviations of axial distance determination are recognizable if the distance between the peaks is changed from $D=600$ to 40 nm. In this simulation algorithm, any noise factors except photon statistics were not taken into account. Figure 6 shows an example for the virtual microscopy simulation of two spectral signature channels ($D=40$ nm).

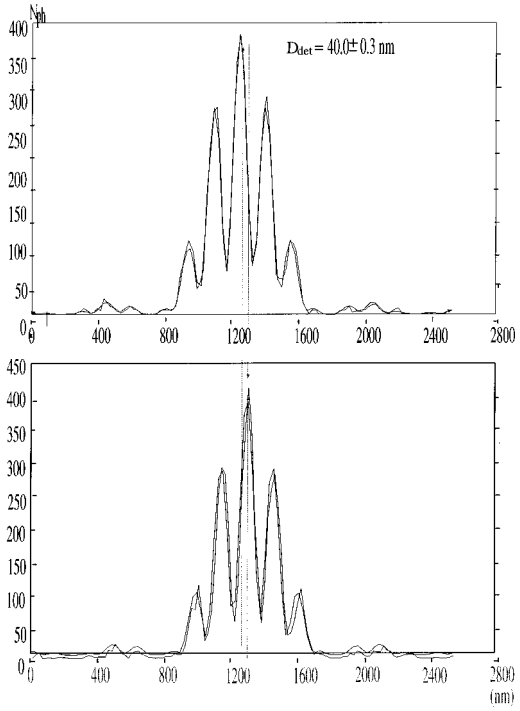

Fig. 6 Virtual axial SMI distance determination. Ordinate: axial object intensity in each channel (for object 1 and for object 2); abscissa: axial position (z/nm). The total number of photons registered per object is $N_{ph}=65\,000$. In this case a "true" distance of $D=40$ nm between the peaks was assumed. A distance D_{det} of (40.0 ± 0.3) nm was determined by the virtual microscopy distance determination algorithm. The two closely overlapping axial intensity curves indicate the simulated axial intensity distribution and the adaptation function, respectively.

8 Summary and Outlook

Here we present the realization of a software for SMI microscopy which allows online visualization of the intensity distributions in the axial and lateral direction for any fluorescent object marked interactively in one of the lateral optical sections. Additionally, statistical parameters can be calculated. This accelerates considerably the potential use of SMI microscopy in biological routine applications, e.g. in genome nanostructure research and generally in molecular cell biology.

Furthermore, results of SPDM using SMI microscopy are presented. Here the precision of axial distance measurements was considered using an absolute distance of 600 nm (i.e. close to the optical resolution limit given by the Rayleigh criterium), and an absolute axial distance of 40 nm (ten times less than the optical resolution). In both cases, two different channels were assumed for the two objects, corresponding to objects with different spectral signatures.[1,2,7,9,19] The simulation results showed that under the assumptions used here the error in distance determination does not increase when decreasing the distance between the point-like objects. In particular, the virtual SPDM SMI simulations shown here indicate that absolute distance measurements down to the 10 nm range with a standard deviation of 1 nm are feasible. To achieve this, a minimum of about 5000 photons have to be detected per object, assuming a ''zero'' background in the region of interest studied.

A precision of distance determination in the range of a few nm may even be realized with less than 1000 detected photons. This provides a way to perform high precision distance measurements even under very adverse photon count conditions, such as encountered in time resolved living cell studies.[21]

Using the SPDM method, distances considerably below 100 nm with standard deviations in the range of 10 nm and better can be obtained using also other microscopical methods, such as conventional microscopy[7] or confocal laser scanning microscopy.[19] However, virtual microscopy simulations (data not shown) indicate that conventional PSFs (as in epifluorescence or confocal microscopy) do not allow nanometer distance measurements at low photon counts and with nanometer precision, whereas this, however, should be possible using PSF engineered microscopy, such as 4Pi,[22] STED, [23] and SMI microscopy.[13]

For example, it is important to measure small condensation changes in specific genes in human cell nuclei.[3,24] Such measurements are possible by spectral precision distance microscopy using different spectral signatures;[2] or even using one spectral signature only, by analyzing the SMI-intensity modulation; in this context, the online visualization procedure described here allows an immediate visual access. A quantitative evaluation procedure of the axial intensity distribution[25] allows also quantitatively valid size determination, down to a small fraction of the exciting wavelength used.

In the future, we may upgrade the software to a variety of different scanning modes, e.g. a lateral scanning during the acquisition process using the stepper motors for automatic measurements of large areas on the object slide. Because of the object oriented structure of the source code, further improvements will be easy to realize.

Acknowledgments

The financial support of the Deutsche Forschungsgemeinschaft and the German Federal Minister of Education, Science, Research and Technology are gratefully acknowledged. B. Albrecht and A. V. Failla contributed equally to this work. The authors thank U. Spöri for stimulating discussions.

References

1. H. Bornfleth, K. Sätzler, R. Eils, and C. Cremer, ''High-precision distance measurements and volume-conserving segmentation of objects near and below the resolution limit in three-dimensional confocal fluorescence microscopy,'' *J. Microsc.* **189**, 118–136 (1998).
2. A. Esa et al., ''Three-dimensional spectral precision distance microscopy of chromatin nanostructures after triple-colour DNA labeling: a study of the BCR region on chromosome 22 and the Philadelphia chromosome,'' *J. Microsc.* **199**, 96–105 (2000).
3. T. Cremer et al., ''Chromosome territories, interchromatin domain compartment and nuclear matrix: An integrated view of the functional nuclear architecture,'' *Crit. Rev. Eukaryot Gene Expr* **12**(2), 179–212 (2000).
4. E. Schroeck et al., ''Multicolor spectral karyotyping of human chromosomes,'' *Science* **273**, 494–497 (1996).
5. M. R. Speicher, S. Gwyn Ballard, and D. C. Ward, ''Karyotyping human chromosomes by combinatorial multi-fluor FISH,'' *Nat. Genet.* **12**, 368–375 (1996).
6. P. Edelmann, A. Esa, M. Hausmann, and C. Cremer, ''Confocal laser-scanning fluorescence microscopy: In situ determination of the confocal point-spread function and the chromatic shifts in intact cell nuclei,'' *Optik* **110**, 194–198 (1999).
7. D. Lacoste et al., ''Ultrahigh-resolution multicolor colocalization of

single fluorescent probes,'' *Proc. Natl. Acad. Sci. U.S.A.* **97**, 9461–9466 (2000).
8. M. Schmidt, M. Nagorny, and S. W. Hell, ''Subresolution axial measurements in far-field fluorescence microscopy with precision of 1 nanometer,'' *Rev. Sci. Instrum.* **71**, 2742–2745 (2000).
9. A. M. van Oijen, J. Köhler, J. Schmidt, M. Müller, and G. J. Brakenhoff, ''3-Dimensional super-resolution by spectrally selective imaging,'' *Chem. Phys. Lett.* **292**, 183 187 (1998).
10. B. Bailey, D. Farkas, D. Taylor, and F. Lanni, ''Enhancement of axial resolution in fluorescence microscopy by standing-wave excitation,'' *Nature (London)* **366**, 44–48 (1993).
11. B. Schneider et al., ''A dual-laser, spatially modulated illumination fluorescence microscope,'' *Microsc. Anal.* **57**(1), 5–7 (1999).
12. B. Schneider et al., ''Nanolocalization measurements in spatially modulated illumination microscopy using two coherent illumination beams,'' *Optical Diagnostics of Living Cells III*, *Proc. SPIE* **3921**, 321–330 (2000).
13. B. Albrecht, A. Schweitzer, A. V. Failla, P. Edelmann, and C. Cremer, ''Spatially modulated illumination (SMI) microscopy allows axial distance resolution near one nanometer,'' (submitted).
14. D. Chapman, *Teach Yourself Visual C++ in 21 Days*, SAMS Publishing (1998).
15. D. Kruglinski, S. Wingo, and G. Shepherd, *Inside Visual C++ 6.0*, Microsoft Press, Redmond (1998).
16. D. Pallmann, *Programming Bots, Spiders, and Intelligent Agents in Microsoft Visual C++*, Microsoft Press, Redmond (1999).
17. A. V. Failla, B. Albrecht, A. Schweitzer, and C. Cremer (in preparation).
18. B. Schneider, J. Bradl, I. Kirsten, M. Hausmann, and C. Cremer, ''High precision localization of fluorescent targets in the nanometer range by spatially modulated excitation fluorescence microscopy,'' *Fluorescence Microscopy Fluorescence Probes*, J. Slavik, ed., Vol. 2, 63–68 (1998).
19. P. Edelman and C. Cremer, ''Improvement of confocal spectral precision distance microscopy (SPDM),'' *Proc. SPIE* **3921**, 313–320 (2000).
20. A. V. Failla and C. Cremer, ''Virtual spatially modulated illumination microscopy predicts nanometer precision of axial distance measurements,'' *Proc. SPIE* (submitted).
21. H. Bornfleth, P. Edelmann, D. Zink, T. Cremer, and C. Cremer, ''Quantitative motion analysis of subchromosomal foci in living cells using four-dimensional microscopy,'' *Biophys. J.* **77**, 2871–2886 (1999).
22. S. W. Hell, E. H. K. Stelzer, S. Lindek, and C. Cremer, ''Confocal microscopy with an increased detection aperture: type-B 4π confocal microscopy,'' *Opt. Lett.* **19**, 222–224 (1994).
23. T. A. Klar, S. Jakobs, M. Dyba, A. Egner, and S. W. Hell, ''Fluorescence microscopy with diffraction resolution barrier broken by stimulated emission,'' *Proc. Natl. Acad. Sci. U.S.A.* **97**, 8206–8210 (2000).
24. T. Cremer and C. Cremer, ''Chromosome territories, nuclear architecture and gene regulation in mammalian cells,'' *Nat. Rev. Genetics* **2**, 292–301 (2001).
25. A. V. Failla et al. (in preparation).